Construction and Building Materials 192 (2018) 272–286

Contents lists available at ScienceDirect

Construction and Building Materials

journal homepage: www.elsevier.com/locate/conbuildmat

Calibration of sonic pulse velocity tests for detection of variable conditions in masonry walls

Maria Rosa Valluzzi [a,*], Elvis Cescatti [b], Giuliana Cardani [c], Lorenzo Cantini [d], Luigi Zanzi [c], Camilla Colla [e], Filippo Casarin [f]

[a] DBC – Department of Cultural Heritage, University of Padova, P.za Capitaniato 7, 35139 Padova, Italy
[b] DICEA – Department of Civil, Environmental and Architectural Engineering, University of Padova, Via F. Marzolo 9, 35131 Padova, Italy
[c] DICA, Department of Civil and Environmental Engineering, Politecnico di Milano, P.za L. da Vinci 32, 20133 Milano, Italy
[d] DABC, Department of Architecture, Built Environment and Construction Engineering, Politecnico di Milano, P.za L. da Vinci 32, 20133 Milano, Italy
[e] DICAM, Department of Civil, Chemical, Environmental and Materials Engineering, University of Bologna, V.le Risorgimento 2, 40136 Bologna, Italy
[f] Expin s.r.l., Via Panà 56ter, 35027 Noventa Padovana, Padova, Italy

HIGHLIGHTS

- Experimental validation of diagnostic methods based on waves propagation on purpose-built masonry specimens.
- Comparison of different methods based on sonic wave transmission on representative types of masonry.
- Optimization of sonic test procedure to identify anomalies in masonry.
- Identification of sonic velocity values of various materials detectable in existing masonry.

ARTICLE INFO

Article history:
Received 14 January 2018
Received in revised form 25 July 2018
Accepted 5 October 2018

Keywords:
Sonic pulse velocity
Direct tests
Tomography
MASW
Brick masonry
Stone masonry
NDT
Calibration
Grout injection
Flaw

ABSTRACT

Sonic pulse velocity is a non-destructive method used for diagnosing existing masonry and evaluating the effectiveness of interventions. A new comparative study is presented here, aimed at checking the reliability of the method in detecting inhomogeneities in order to qualify various masonry conditions, according to common practice and up-to-date tools, for both on-site testing and data handling. Four research groups applied direct and tomographic sonic velocity tests on three full-size wall specimens representing existing masonry types. The surface wave method was also applied to one of the specimens, to compare various outputs of elastic wave transmission. The panels incorporated various flaws and inclusions and were consolidated by grout injections. Each research unit applied its own acquisition systems and processing methods before and after panel consolidation. The results confirmed the ability of sonic pulse velocity tests in detecting large inclusions and significant variations in compactness, and provided quantitative reference values for materials and conditions. The research provided directions for further optimization of sonic waves transmission test application in already existing masonry constructions.

1. Introduction

The preservation of architectural heritage requires primary implementation, in the diagnostic phase, of a knowledge process based on visual inspection and experimental procedures [4]. In such a context, the correct application of Non-Destructive Testing (NDT) methods is crucial in evaluating the current conditions of materials and structural components without affecting their integrity [3]. Among NDT methods, the Sonic Pulse Velocity Test (SPVT) is commonly applied to existing and historical structures to evaluate the quality of masonry. The method applies the transmission of elastic waves (range of frequency domain 20 Hz–20 kHz) between couples of measurement stations located at known distances on the wall surface [1,22,24,17,11]. An elastic mechanical impulse is generated by an instrumented hammer striking the surface of the material, and the propagated signal is then received by one or more accelerometers. For each travel time the signal transmission velocity is computed according to the assumed minimum distance (straight-line path) between each

* Corresponding author.
E-mail address: mariarosa.valluzzi@unipd.it (M.R. Valluzzi).

https://doi.org/10.1016/j.conbuildmat.2018.10.073
0950-0618/

couple of stations. Heterogeneities, voids or inclusions of other materials would change the wave path, as sonic waves tend to travel faster in denser materials (minimum speed value refers to propagation in air). Consequently, as wave velocity is a qualitative indicator of the density of the study material, the method compares compactness variations in order to identify unknown conditions inside the material and can thus evaluate its state. Direct configurations of measurement points (source and receiving stations face each other on opposite wall sides) and tomographic extension (combination of crossing signal paths involving at least two sides of a wall section) are mostly used in real-life investigations. They both refer to the first arrival of longitudinal, primary (P) waves, the fastest among those generated by impact (including, e.g., shear and Rayleigh waves) and are therefore particularly suitable for identifying and locating inner anomalies [16,23,6,20]. Signals are collected at a regular mesh of points marked on the masonry surface, and the computed set of velocities can then be post-processed by software for mapping values distributed over the study area. More recently, another method based on elastic wave propagation, called MASW (Multichannel Analysis of Surface Waves), has gained popularity in similar applications on various scales [28,19]. MASW is based on the interpretation of the dispersion characteristics of surface waves generated by a hammer. Applying MASW to masonry structures is also promising, since the dispersion characteristic of these waves is more pronounced when the medium is highly heterogeneous. Miranda et al. [21] compared direct, indirect and impact echo tests, and evaluated a relationship between the measured wave forms (P and Rayleigh waves) influenced by the presence of mortar joints.

However, regardless of method and data processing, tests based on wave transmission may present a series of uncertainties, particularly in highly non-homogeneous materials such as historic masonry, with a rather high approximation. Therefore, sonic tests should be part of a more extensive experimental diagnostic plan, including other test methods, properly cross-checked to confirm and/or validate results [7–9,5,15,13,34]. Masonry being a composite material, due to its heterogeneity and the extreme variety of types, measured elastic wave velocity values cannot be correlated with physical or mechanical properties (e.g., mass density, Young's modulus). However, the ranges of velocity variation can indicate the condition of the wall [18,3,25,5], with results which are effective in comparing the varying conditions of the material in the building. Hence, sonic velocity figures can identify weak areas, such as those requiring possible intervention, or can quantify the effectiveness of consolidation, e.g., in the case of grout injections [26,12,32,33,27]. According to [3], average sonic velocity exceeds 2000 m/s for good-quality brick masonry (or 2500 m/s for stone masonry, according to [18]). For medium-quality masonry, velocity ranges between 1000 and 2000 m/s (or 1500–2500 m/s), with values below 1000 (or 1500) m/s for poor-quality masonry. Successful grout injections, capable of filling medium-large voids in injectable masonry, can easily raise the velocity to that of solid, good-quality masonry; the average velocity increase after grouting ranges from 40% in real-life applications [8] to about 2.5 times in experimental laboratory tests [33,27].

Several other aspects may affect sonic test results: (a) the testing equipment, (b) on-site application and acquisition phases, and (c) data processing assumptions [16,10]. In order to investigate still open issues on the sonic test procedure for calibrating and identifying various conditions in masonry structures, an experimental laboratory program was organized among research units (RUs) from the University of Padova, Politecnico di Milano, University of Bologna and the University of Padova's spin-off Expin srl. Research compared the reliability of sonic tests performed by the RUs on a series of specimens reproducing various types of masonry and cross-sectional conditions. MASW tests were also carried out on one specimen. Three three-leaf full-sized panels (about $120 \times 120 \times 40\ cm^3$, length x height x thickness) were purpose-built to serve as physical models for all the RUs. The specimens consisted of outer leaves made of fired-clay solid bricks, rubble stones or a combination of both (i.e., stonework regularized by cross-through brick courses) and an incoherent inner core. Wall designs anticipated a series of anomalies representing voids or inclusions (e.g., plastic pipes, steel tie rods, pieces of timber). In addition, in a later phase, the inner cores of the specimens were improved with grout injections.

In this paper, results are compared in terms of differing wall conditions but also specific acquisition systems, modes of application and processing methods adopted by the RUs. The application to the same specimens and all data shared among the RUs also allowed quantitative evaluation of the sonic velocity values representative of the various materials and the variable states detectable in existing masonry constructions.

2. Experimental campaign

The experimental campaign involved four experienced research units from the University of Padova (RU1), Politecnico di Milano (RU2), University of Bologna (RU3) and Expin s.r.l. (RU4). To reproduce and compare current application methods of sonic tests to masonry, all the RUs, according to their current in-situ practice, used their own equipment, data acquisition systems and post-processing tools on a set of three multi-leaf masonry panels. Each RU applied SVPT to the three specimens in turn, so that the results could be compared in the same conditions. The specimens were purposely designed and built with some inclusions (e.g., a timber element, transverse connections made of anchored steel ties or bricks, a pipe simulating installations) and other irregularities. In order to reproduce vulnerable masonry conditions in both vertical and horizontal (e.g., seismic) loads, the three-leaf section walls were built with weak inner cores. The external layers represented common types of layouts for existing masonry constructions, i.e.: a multi-type rubble stone pattern including a solid section of brick courses (P1-M), a regular fired-clay brick pattern (P2-B) and a rubble stone pattern (P3-S). In a later experimental phase, in order to improve the overall compactness of the walls, the inner incoherent layers were filled with grout. Direct sonic tests and sonic tomography (across horizontal and vertical sections) were then carried out on the walls before and after consolidation. In addition, on specimen P2-B, the applicability of the MASW method at sonic scale was tested, in order to evaluate the effectiveness of grout injections along a bisector of the panel.

2.1. Specimens

Rubble limestone elements of irregular shapes and dimensions from the Cugnano quarry (Belluno, Italy) [31] were used for construction of specimens P1-M and P3-S; standard commercial fired-clay solid bricks ($12 \times 5.5 \times 25\ cm^3$) were used for P1-M and P2-B. Two natural hydraulic lime-based mixes were used for the panels, one for mortar joints and the other (calibrated with proper fluidity) for grout injection. During construction, the inner cores of the walls were filled with gravel and flakes, the latter made of the same stones as the single walls. Each specimen rested on a reinforced concrete base to facilitate handling (Fig. 1).

Specimen P1-M ($114 \times 127 \times 37\ cm^3$) was made of rubble stone masonry whytes with an incoherent core (each crossing at about one-third of thickness of the wall), with their upper and lower parts separated by four brick courses crossing the entire thickness of the wall; Fig. 1a). These courses are sometimes found in existing irregular stone masonry, to regulate compression

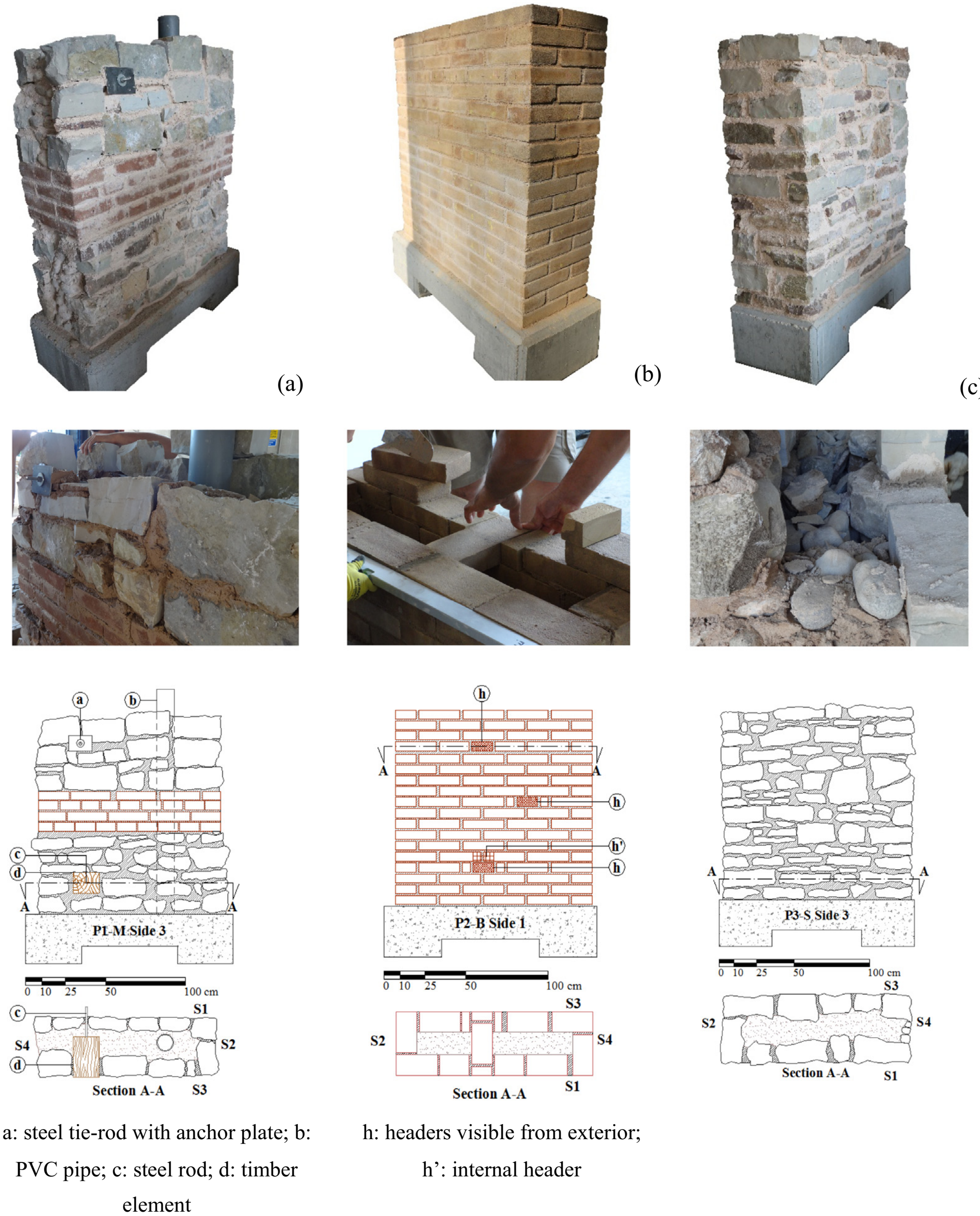

Fig. 1. Overall view of specimens and details of construction: (a) multi-type wall P1-M, (b) brick wall P2-B, (c) stone wall P3-S.

stresses acting along panels and to connect external whytes locally. A vertical PVC pipe (diameter 110 mm) ran in the inner core for the whole height of one side of the wall, creating a cylindrical void simulating the passage of a drainpipe or other systems. On the opposite end of the wall, a transverse steel tie rod (diameter 12 mm), anchored outwards by a steel plate ($145 \times 100\ mm^2$) was placed in the upper part of the panel. A timber beam element ($160 \times 130\ mm^2$) with a centrally placed steel rod (6 mm in diameter) was positioned in the lower wall portion.

Specimen P2-B ($120 \times 120 \times 39\ cm^3$) was made up of two external one-head-thick brick whytes with a regular layout and mortar joint thicknesses ranging from 1 to 1.5 cm (Fig. 1b). Four brick headers, acting as shear elements connecting front and rear wall whytes, were placed round the central vertical line of the panel at the 4th, 9th, 14th and 15th courses from the top, alternating at the two sides.

Specimen P3-S ($126 \times 125 \times 45\ cm^3$) was made of two rubble stone leaves and an incoherent core, each spanning about one-third of the section thickness (Fig. 1c). Due to the irregularity of the stone courses, the mortar joints in this panel had variable thicknesses, generally not exceeding 2 cm.

In a second measurement campaign, both P2-B and P3-S panel cores were fully consolidated with grout injections. In the P1-M wall, in order to compare sonic test results applied on injected and non-injected portions directly, only the lower part of the wall - below the brick courses – was consolidated. The injection grout was a ready-to-mix product; however, in order to optimize its rheological properties, preliminary fluidity [2] and injectability tests were performed [30]. According to the results, a water/mix ratio of 0.4 by weight was adopted. The panels were injected from one front only, slowly progressing from the base to the top of the walls, by means of a manual system of combined pump and mixer (Fig. 2). To reach the core, a 12-mm diameter drill bit was used to bore a series of holes through the thickness of the external whyte, according to a triangular mesh with sides of 30–40 cm.

Fig. 2. Injection phase of panel P3-S (a) and rising grout in panel P2-B (b).

The holes were slightly inclined downwards, in order to optimize grout percolation in the core. On the back of the panels, a few additional (non-injected) control holes allowed monitoring of grout migration. Plastic hoses (external and internal diameters of 12 and 9 mm, respectively) were inserted into the drilled holes and used as grout inlets. The whole injection process was monitored in terms of grout quantities, from one hole to the next, and any possible grout outflows were promptly sealed after any rise of grout in the hoses was seen (Fig. 3) (Table 1). For the P1-M panel, the solid brick courses provided an effective barrier against upward grout migration.

2.2. Investigation program

Each RU approached the panels for the direct, tomographic or MASW tests, according to their usual procedures, before and after injections. Pre-injection sonic tests were performed from 30 to 90 days after panel curing; post-injection tests started 60 days after injection. Table 2 lists the geometric characteristics of the meshes adopted by the RUs for direct and tomographic tests. All four RUs made direct tests on all three panels, according to grids of corresponding points on the two opposite main faces of the specimens. RU2 and RU3 did not generally include the full thickness at the vertical edges of walls; RU1 and RU4 extended their tests to larger surfaces, which would also account for the edge effect. However, all RUs had quite small-spaced meshes, taking into account the textural variety of the walls (especially for panel P1-M) and facilitating more precise results. RU3 also applied direct tests to specimen P1-M, with a mesh of 11 × 6 points spaced at 10 cm, to study the lower portion of the wall only (the one subjected to injections). Fig. 4 shows the overlap of the investigated areas for direct tests by the RUs.

Tomography was applied to horizontal cross-sections of all three specimens (four sides, by RU1, RU2, RU3; two sides by RU3) (Fig. 5) and vertical sections to P1-M and P2-B walls only (two sides, by RU1 and RU3, both using the same configuration of station of points along 110 cm in the mid-panels, although with a different number of wave paths) (Fig. 6a). The MASW test was applied along the bisector line of P2-B panel (RU2) at 12 points, spaced at 9 cm and covering a total spread length of about 1 m (Fig. 6b); no brick headers were crossed by the test line, thus the effect of consolidation of the inner core was compared with the sonic test results.

2.3. Testing equipment and processing tools

To check any variability of results according to differences in acquisition and processing tools, each RU adopted hardware and settings commonly used on-site on masonry structures. RU1's equipment was composed of a hammer with a 1.1 kg mass and a hard plastic tip (51 mm diameter), instrumented with a piezometric load cell with sensitivity of 0.23 mV/N, the response curve of which provided a frequency range of 700–1050 Hz, from 5 to 20 dB, on the tested materials (Fig. 7a). Piezometric accelerometers, sensitivity

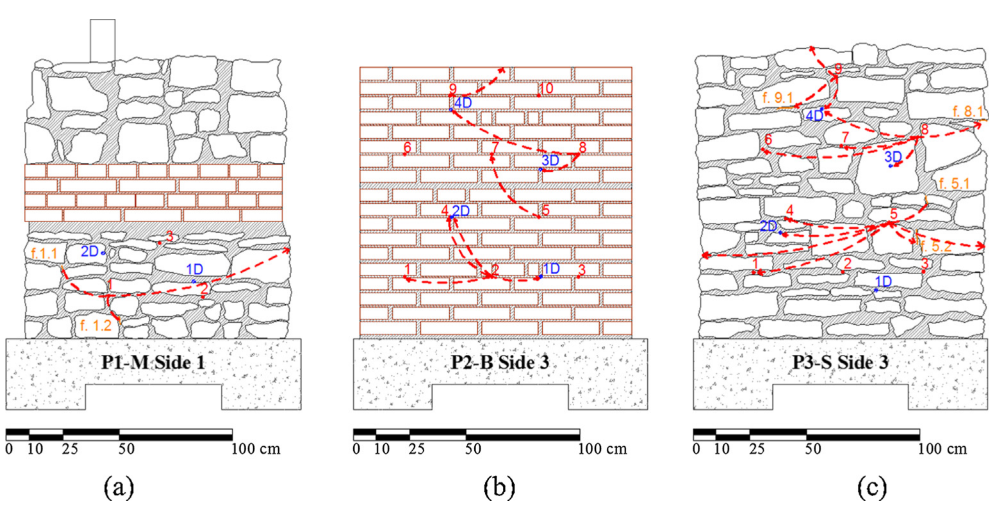

Fig. 3. Progressive grout migration in specimens (a) multi-type wall P1-M, (b) brick wall P2-B, (c) stone wall P3-S (numbers: position of injection holes and progressive flow of grout, according to arrowed paths).

Table 1
Quantity of grout injected in specimens and computed percentage of voids in cores.

Specimen		P1-M	P2-B	P3-S
Dimensions (l × h × t)	(cm^3)	114 × 52 × 37	120 × 120 × 39	126 × 125 × 45
Core thickness (approx.)	(cm)	13	14	15
No. of injection holes		3	10	9
No. of control holes		2	4	4
Quantity of grout injected	(lt)	13.4	31.8	90.0
Percentage of voids in core	(%)	17.3	15.8	38.1
Overall void percentage in walls	(%)	6.1	5.7	12.7

Table 2
Main testing configurations applied by RUs.

Research unit	Specimen	Direct tests		Tomographic tests	
		Tested area (cm^2)	Mesh spacing (cm^2)	Horizontal (no. of points)	Vertical (no. of points)
RU1	P1-M	90 × 90	10 × 10	4 × 11	11
	P2-B	90 × 80			
	P3-S	90 × 90		–	–
RU2	P1-M	75 × 75	15 × 15	1 × 7	–
	P2-B			1 × 8	
	P3-S				
RU3	P1-M	90 × 90	10 × 10	0 × 11	11
	P2-B	100 × 80			
	P3-S	110 × 100		3 × 10	–
RU4	P1-M	100 × 100	10 × 10	–	–
	P2-B	80 × 80			
	P3-S	110 × 110			

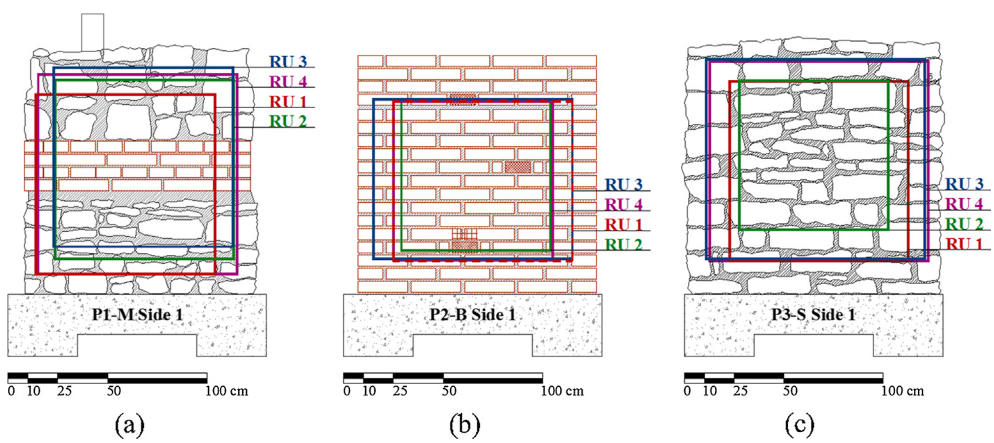

Fig. 4. Direct sonic tests: overlapping of areas tested for (a) multi-type wall P1-M, (b) brick wall P2-B, (c) stone wall P3-S.

10000 mV/g and resolution 0.000008 g ms, were used as receivers. The acquisition system was an integrated PXI-1025 system with PXI-4472 modules, with a sampling frequency of 102.4 kS/s. A signal sampling frequency of 50 kHz was used. Three signals were acquired at each test station with a CoV of 10% between each velocity value along the same path. Travel time was computed by an automatic algorithm implemented in the Labview environment [14]. Tomographic configuration allowed simultaneous acquisitions of seven accelerometers per impact. In-house software based on straight ray paths was used for tomographic processing.

RU2 performed sonic pulse velocity tests with an instrumented hammer with an aluminium tip (8 mm diameter) and a load cell of 4.48 kN, providing frequency content of signals around 4.5 kHz, and an accelerometer (Fig. 7b). Signals were acquired at a sampling rate of 20 μs by a National Instrument card connected to a portable PC and recorded by in-house software implemented in Labview [10]. Signals were checked directly by a user-friendly interface; one value (presumed to be the most reliable) per measurement station was recorded. For tomographic elaborations, GeoTomCG commercial software based on curved ray paths was used. For application of the MASW, a hammer equipped with an accelerometer connected to the triggering input of the recording device was used. Lamb-Rayleigh waves were generated in a proper frequency range. Receivers consisted of 12 piezoelectric sensors, fixed with metal springs on L-shaped aluminium elements pasted on the brick surface (Fig. 7c). Since the expected investigation depth of a MASW survey is about half the spread length [29], the covered distance of about 1 m was sufficiently long to explore the whole depth of the specimen section (39 cm thick for P2-B). The expected resolution was about half the receiver spacing, i.e., 5 cm, which was enough to detect the three-layer bricks-core-bricks structure. The possible velocity ranged from 200 m/s in the core before injections to 1500 m/s in the external brick layers (Rayleigh waves travel at about 0.9 the velocity of shear waves), a rough estimate of the frequency bandwidth needed to detect three layers with about the same thickness (i.e., 13 cm) was 200–4000 Hz. This is a frequency

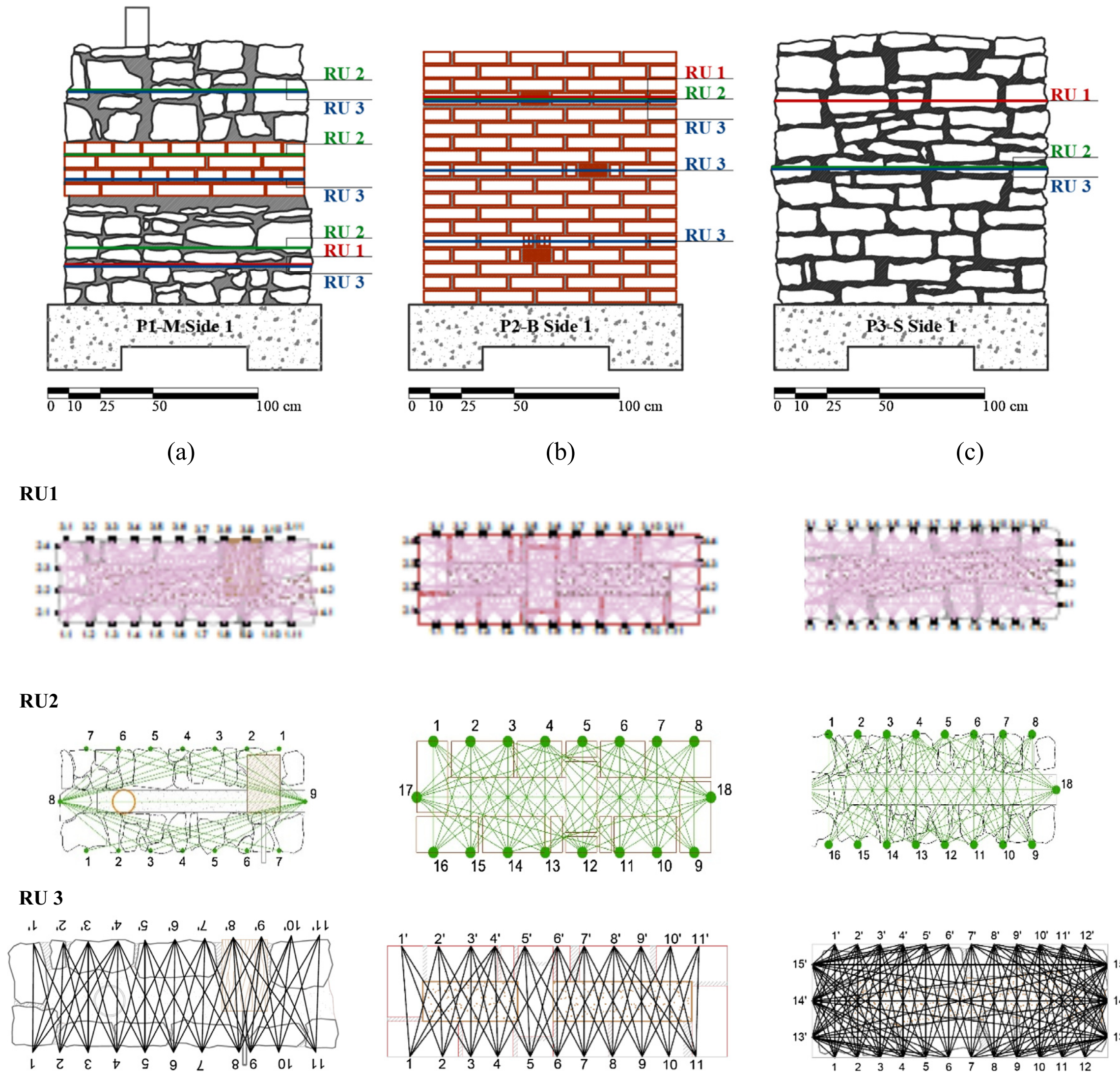

Fig. 5. Sonic tomography on horizontal sections: tested areas and ideal signal paths for (a) multi-type wall P1-M, (b) brick wall P2-B, (c) stone wall P3-S.

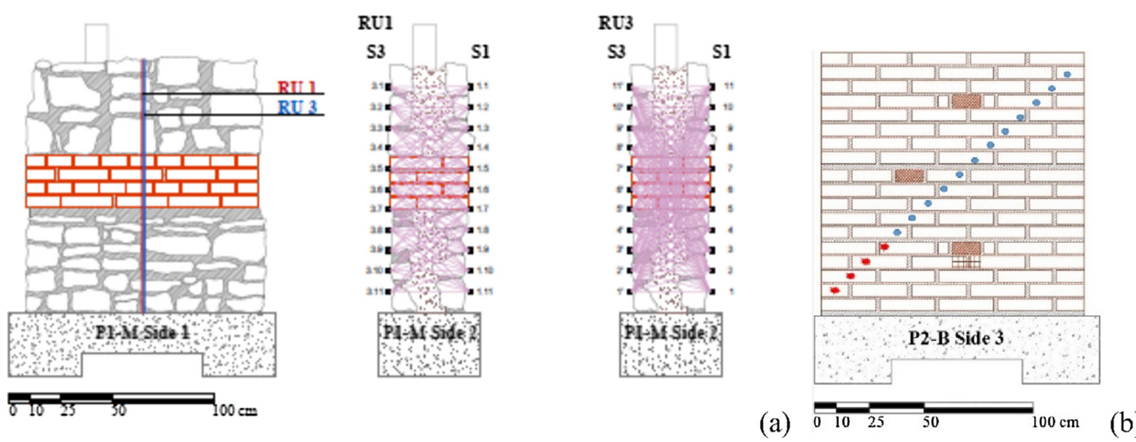

Fig. 6. Sonic tomography on vertical sections: areas studied for multi-type wall P1-M (a). MASW test on panel P2-B (b) (blue: spread of sensors; red: impact positions). (For interpretation of the references to colour in this figure legend, the reader is referred to the web version of this article.)

range which can easily be generated with a small hammer and be received with enough energy at a distance of about 1 m. The recording unit was a 24-channel seismograph from Geometrics (GEODE model). Data were sampled at the highest sampling rate of the seismograph (48 kHz). Four shots were recorded by hammering the specimen surface at different distances from the

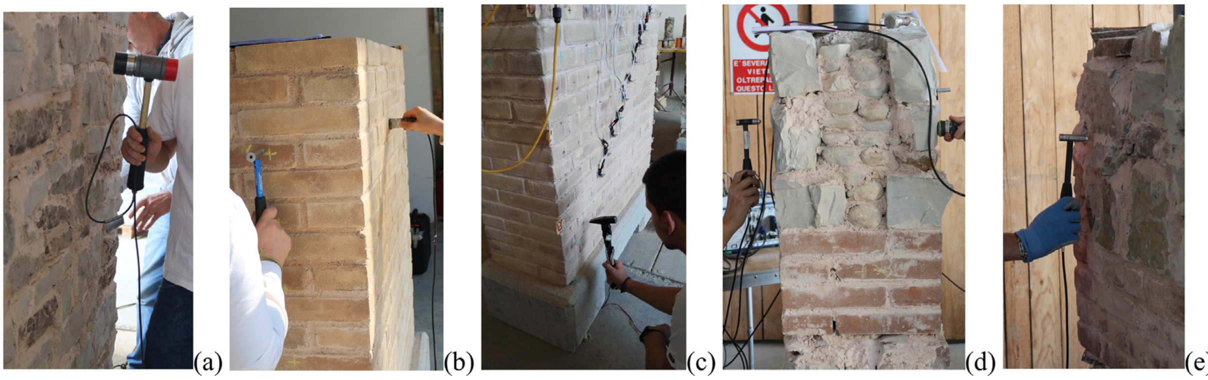

Fig. 7. Sonic data acquisition equipment used by RU1 (a), RU2 for sonic (b) and MASW (c) tests, RU3 (d), and RU4 (e) (hammer and/or receiver sensors).

closest (lower) sensor (Fig. 6b). The dataset was analysed with WinMASW, a commercial software specifically developed for MASW data inversion.

The sonic equipment used by RU3 included a small impact hammer (mass of 0.1 kg and an alloy tip of 6 mm diameter) and sensitivity of 11 mV/N, featuring an integrated high-sensitivity force sensor for amplitude and frequency contents, together with accelerometers as receiving probes with linear response in the region of interest of the spectrum (Fig. 7d). Waveforms were recorded by a PC equipped with a very high-frequency acquisition card. In-house software in Labview environment was used for checking real-time quality signals prior to data recording. Measurement number was limited to one per reading point or more, if necessary. On the materials tested in this experimental work, the generated signals showed maximum frequency between about 1750 Hz and 6650 Hz. In-house data recall and visualization software, as well as commercial software, were used for manual travel-time picking and tomographic inversions, respectively. The latter uses a SIRT algorithm performing both straight-line and curved waveform path iterations.

RU4 used a small hammer of mass 0.16 kg and alloy tip of 6-mm diameter, instrumented by a piezometric load cell with a sensitivity of 2.25 mV/N (Fig. 7e). Receivers, acquisition systems and settings were the same as those for RU1. Travel times were manually detected and displayed by in-house software implemented in Labview.

Table 3 compares acquisition parameters and hammer capacities for the various systems applied to brick or stone masonry specimens.

3. Results and discussion

The various choices made by the RUs resulted in slightly different areas covered by direct tests and different resolutions of both acquisition meshes and processed maps in tomography. Therefore, comparison of the results of direct tests was performed by examining only the common areas investigated by all RUs on panel surfaces, and a uniform definition of the processed meshes was proposed among the RUs for tomography. The following sections describe the main results of direct and tomographic tests applied to the three masonry panels in contour map images of values computed on the mesh areas.

3.1. Direct tests

Direct tests gave significant results in identifying large variations in compactness along the cross-sections of the multiple-leaf walls and evaluating the effectiveness of injections. Results were consistent among all the RUs, as shown in Figs. 8, 9 and 10, which compare the results with respect to the same range of velocities for the contour maps. The most significant aims in pre-injection conditions were achieved, i.e., identification of various masonry materials, brick headers and large cavities, for P1-M, P2-B and P3-S specimens, respectively. The results for panel P1-M show edge effects due to the closeness of the concrete beam at its base and the low position (compared with the other panels) of acquisition meshes, to allow the injected portion of the wall to be examined (Fig. 4a). A similar effect was detected for panel P3-S on the vertical full-thickness edges by all RUs except RU3, whose acquisition mesh purposely did not include borders in order to enhance evaluation of injection effectiveness (Fig. 4c). These interferences in wave transmission affected the average sonic velocity values, as shown in Table 4, which may indicate that, in practical applications, investigations near boundaries of 1–1.5 times the wall thickness should be avoided.

In spite of the denser grid meshes used by some of the RUs, the low resolution of generated signals compared with the size and nature of the inclusions impeded the accuracy of results in the pre-injection state, so that smaller inclusions (e.g., timber elements and PVC pipes) were not identified. However, comparison of velocities computed on specific points gave significant results in terms of quantification of representative average values for as-built masonry (Table 4: missing values correspond to outside tested area points). Consistently average RU values were obtained for all elements (maximum CoV 18%), except for a few out-of-range peaks of velocity in panel P2-B. In particular, RU1 detected a peak for

Table 3
Acquisition parameters and maximum frequency of impulses on basic wall materials.

Parameter		RU1	RU2	RU3	RU4
Sampling frequency (Hz)		50,000	51,200	500,000	50,000
Sampling time (s)		0.00002	0.00002	0.000002	0.00002
Sample number		4096	1260	10,240	4096
Waveform length (s)		0.082	0.025	0.020	0.082
Max frequency (Hz)	Brick	794	2302	2315	2056
	Stone	668	4496	4017	3423

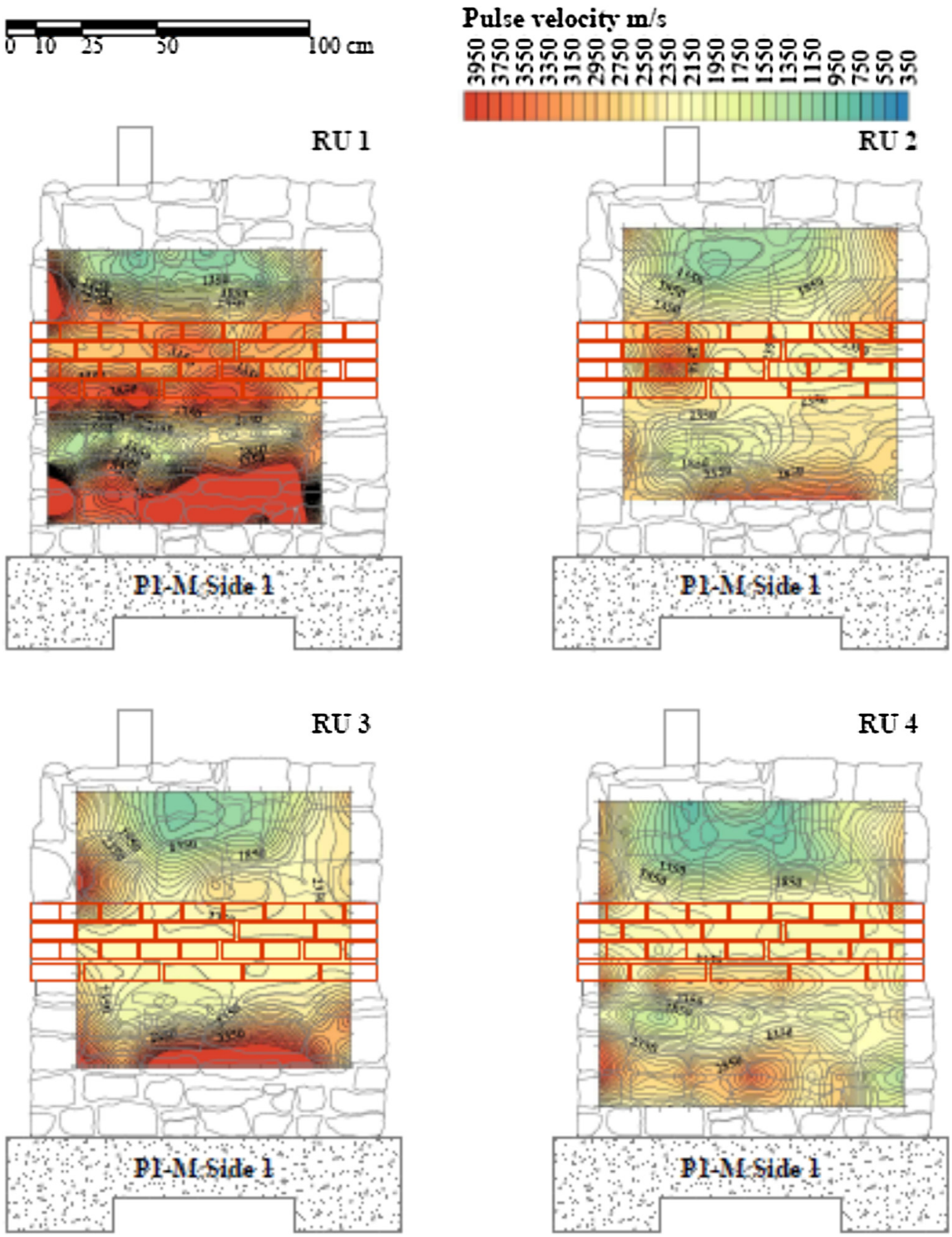

Fig. 8. Direct velocities in panel P1-M before injection: contour maps of various masonry materials (irregular stone leaves and rubble core, solid layer of brick courses) and their conditions (low-density core in upper part of wall and just below brick courses).

transverse brick headers and RU3 for full brick thickness at the edge. This indicates the higher reliability of multiple measures on the same area (minimum CoV of 4%) and the influence of the extent of the area in which the presence of various objects may affect the value (CoV higher than 30%). As expected, the lowest velocity values were those of the incoherent inner core, regardless of the material of the outer layers (stones or clay bricks), and the highest values were those of solid elements (timber, full-thickness stone, or bricks/headers). The variability of these results was not overall high (less than 40%, when the highest singularities were removed) and were due to device calibration and set-up sensitivity.

Table 5 compares the results obtained in study areas in common among all the RUs, before and after injections of the panels (missing values for RU3 are due to the different areas tested before and after injection). All RUs recorded remarkable improvements in the sonic velocity values provided by grouting. Fig. 11 shows some examples of the most significant cases. The most evident results in terms of intervention effectiveness appear in P3-S (Fig. 12), due to the extended volume of the injectable core, unlike P1-M and P2-B, in which inner elements obstructed smooth, regular grout migration inside the wall (also, in the case of P1-M, the injectable core portion was narrower; see also Table 1). Nevertheless, consolidation was able to homogenize the sections of all specimens: core material density improved, as measured by the increase in velocity, with consequent expected positive effects on overall structural performance. This was confirmed by the fact that inner high-density anomalies could not be distinguished, examples being brick shear elements in P2-B after grouting (Fig. 11), where a significant decrease in the CoV was also recorded after injection (Fig. 12). Unlike high-density inclusions, after core injection any

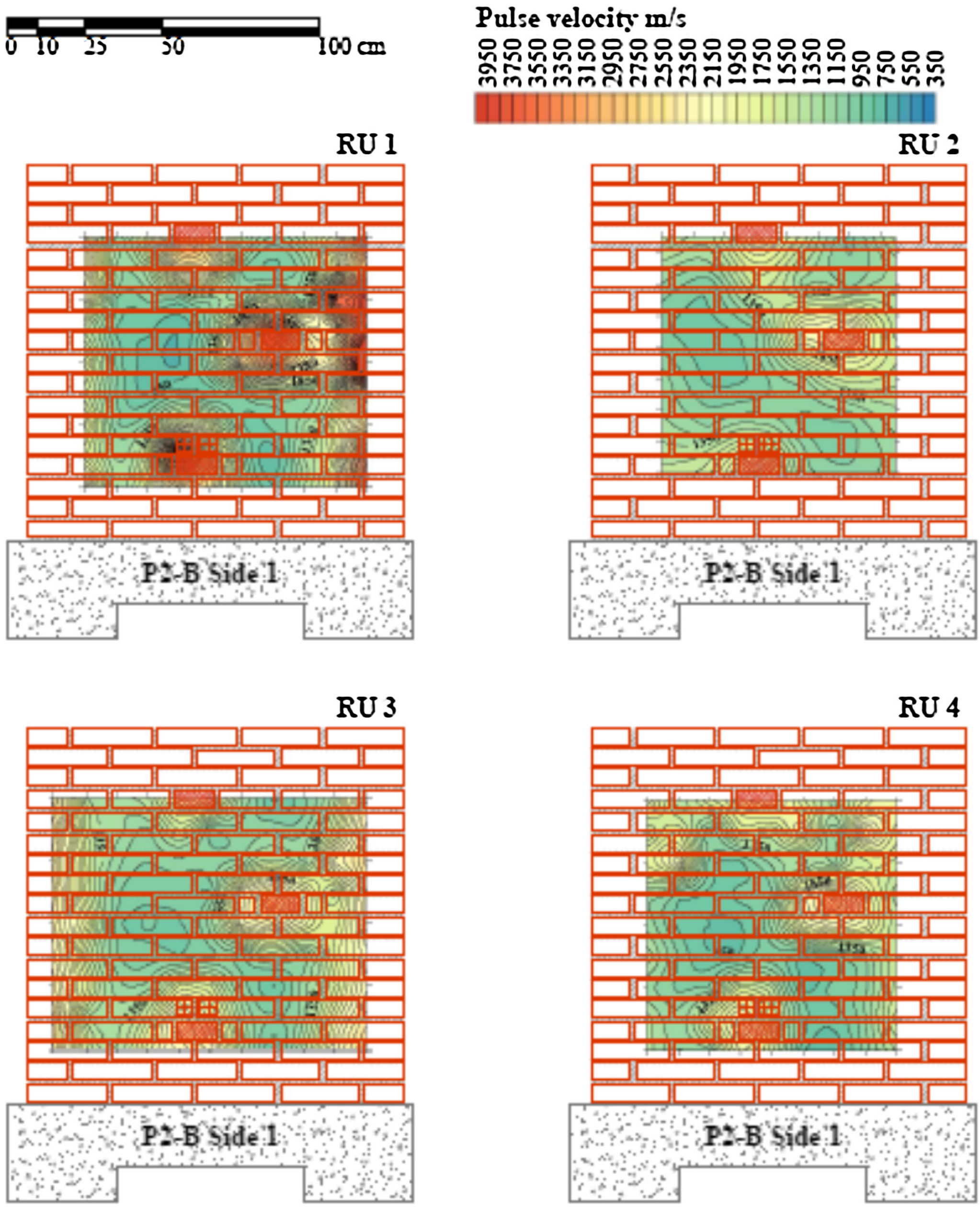

Fig. 9. Direct velocities in Panel P2-B before injection: contour maps clearly identify position of brick headers placed as shear connecting elements.

low-density elements still present became more visible on the map: in the lower portion of P1-M (Fig. 11), the low-velocity areas were clearly visible at both PVC and timber element positions. Before injection, density contrast and therefore the difference in signal propagation velocity between these materials and the core was insufficient to detect these items clearly.

MASW results are traditionally represented by a 1D shear velocity model which describes the layered structure resulting from surface wave inversion. Surface wave velocities are converted into S-wave velocities, assuming that their ratio is 0.9. The basic assumption is that surface waves are dispersive, i.e., their velocity is frequency-dependent. Since each frequency explores a different range of thickness of the material (i.e., high frequencies penetrate less than low frequencies), the velocity versus frequency plot (dispersion curve) can be transformed into a velocity versus depth model. Fig. 13a shows an example of a dispersion curve obtained on specimen P2-B before core injection. The velocity-frequency spectrum is dominated by a fundamental mode from about 400 to 2400 Hz. Although a possible higher mode seems to appear at about 1000 Hz and higher, analysis was limited to the fundamental mode, which shows better resolution and a higher signal-to-noise ratio. Fig. 13b and c show the resulting models obtained before and after injections, due to picking and inverting the dispersion curves in the 400–2400 Hz and 400–3500 Hz frequency ranges, respectively. A larger frequency range in the post-injection situation is the direct consequence of the lower absorption of the injected core compared with that of the pre-injection filling material. The pre-injected model (Fig. 13b) clearly identified the core of a low-velocity material within specimen P2-B. A contrast of 360 m/s versus 1450 m/s was observed between the low-velocity core and the brickwork. The second model (Fig. 13c) showed a significant increase in velocity inside the wall core (from 360 to 750 m/s), which proves the general effectiveness of core injections.

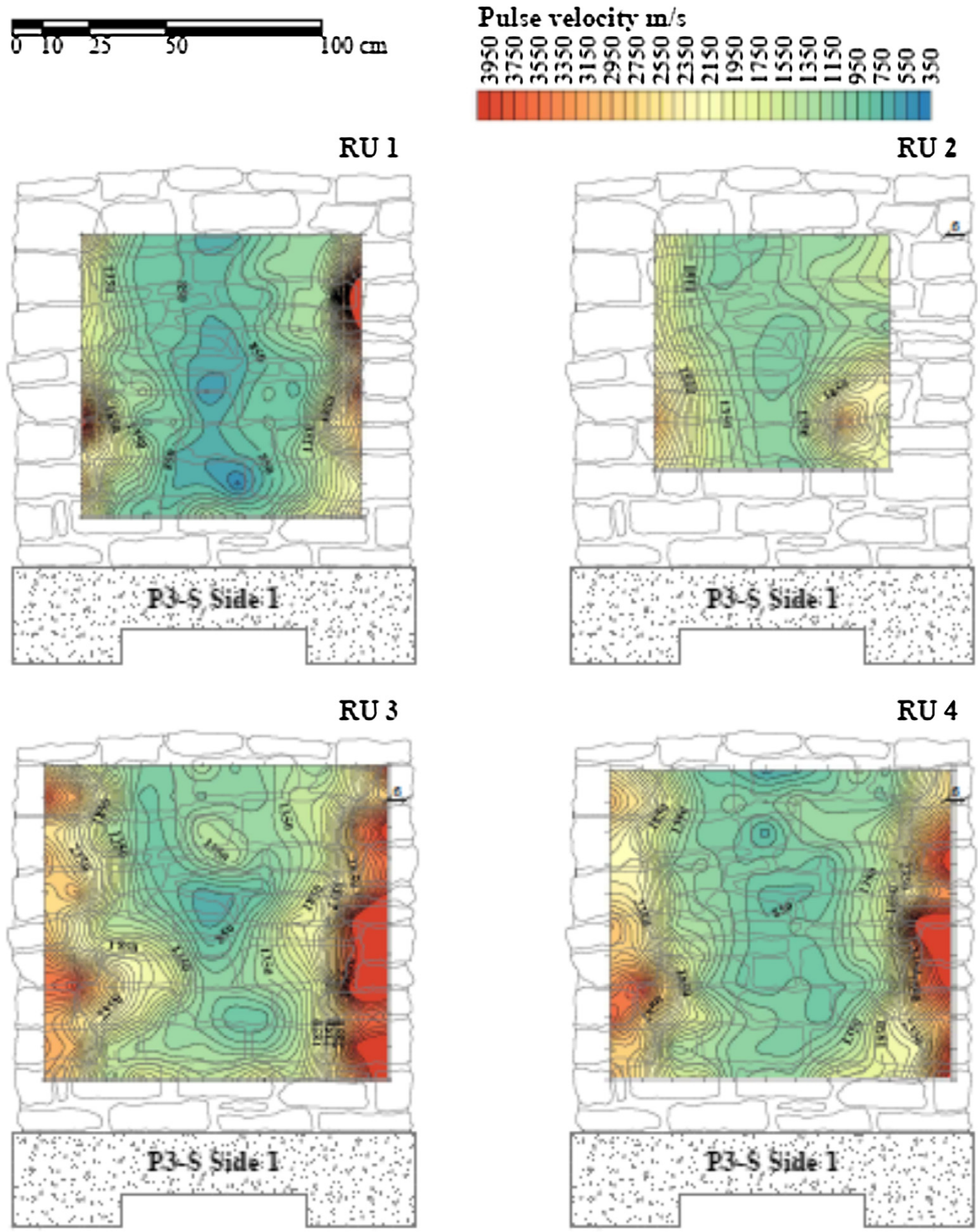

Fig. 10. Direct velocities in Panel P3-S before injection: contour maps identify large incoherent core in comparison with full stone thickness at left and right borders.

Table 4
Average values of velocity computed by direct tests on wall elements.

Specimen	Object	Direct test velocity (m/s)				Average velocity (m/s)	CoV (%)
		RU1	RU2	RU3	RU4		
P1-M	Timber element	3132	3750	4348	3126	3589	16
	Full stone thickness (border)	2864	2682	3553	2566	2916	15
	Full brick thickness	3289	2830	2256	2566	2735	16
	Inner core (intersecting stone whytes)	1966	2417	2494	1818	2174	15
P2-B	Full brick thickness (border)	3330	–	4019	3290	3546	51
	Transverse brick headers	4221	2313	2103	2597	2809	34
	Inner core (intersecting brick whytes)	1350	1271	1393	1373	1347	4
P3-S	Inner core (intersecting stone whytes)	1237	1212	1740	1574	1441	18

Assuming rough estimation of Poisson's ratios of 0.3 for the core before injections and 0.2 for bricks and core after injections, S-wave velocities were converted into P-wave ones and compared with results from direct sonic tests. P-wave velocities turned out to be about 2400 m/s for the brick layers, and 700 and 1200 m/s for the pre- and post-injected core materials, respectively.

Table 5
Average velocity detected before and after grout injection and improvement ratios (CoV in brackets).

Specimen	Velocity (m/s)	RU1	RU2	RU3	RU4
P1-M	Before	2874 (38%)	2778 (28%)	2645 (36%)	2202 (29%)
	After	3352 (38%)	3623 (18%)	3451 (–)	2535 (28%)
	Improvement ratio	25% (45%)	26% (173%)	30% (–)	17% (18%)
P2-B	Before	1674 (47%)	1358 (29%)	1455 (31%)	1413 (32%)
	After	2211 (33%)	1906 (18%)	2332 (18%)	2047 (18%)
	Improvement ratio	51% (47%)	48% (26%)	60% (31%)	57% (33%)
P3-S	Before	1237 (51%)	1560 (37%)	1753 (50%)	1547 (50%)
	After	4439 (14%)	3270 (11%)	3777 (13%)	3661 (12%)
	Improvement ratio	321% (39%)	132% (31%)	115% (41%)	181% (37%)

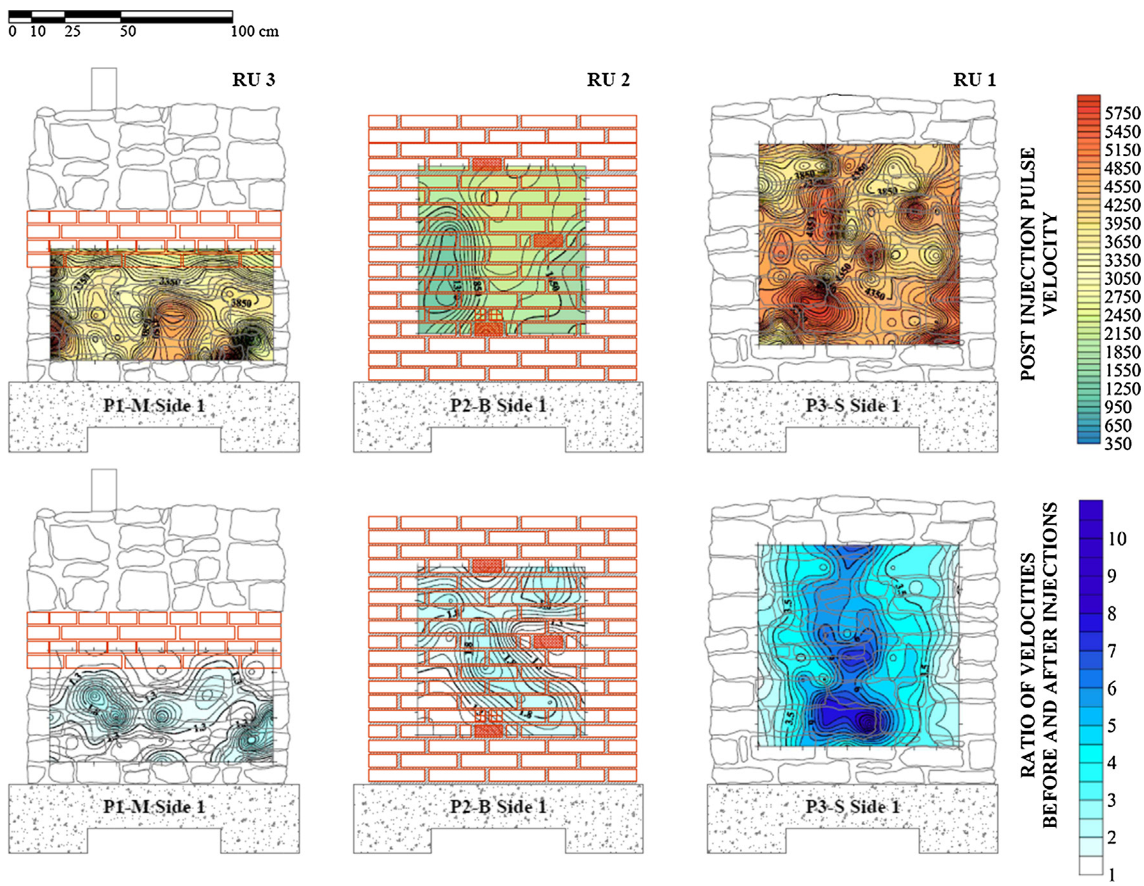

Fig. 11. Example of post-injection results: sonic velocity increased significantly in injected wall portions, particularly for wall P3-S.

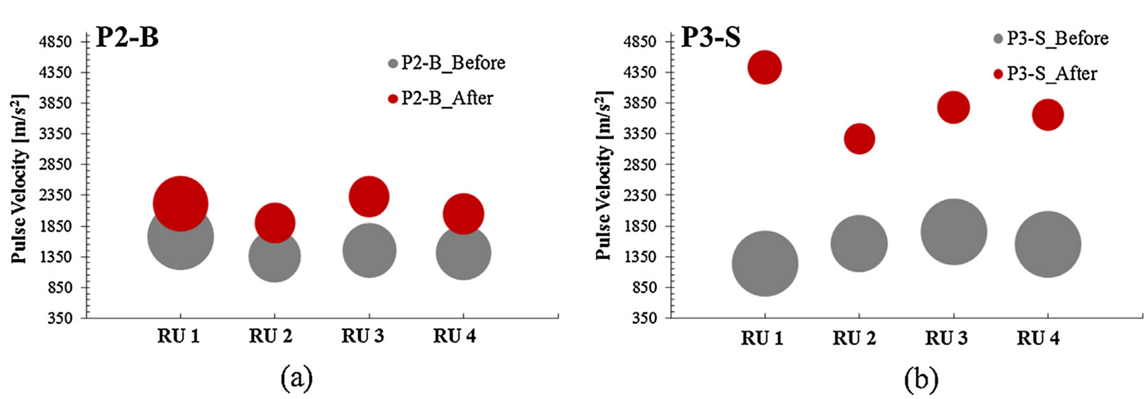

Fig. 12. Comparison of effectiveness of injection for P2-B (a) and P3-S (b) panels grouted in whole core (size of circles: CoV values).

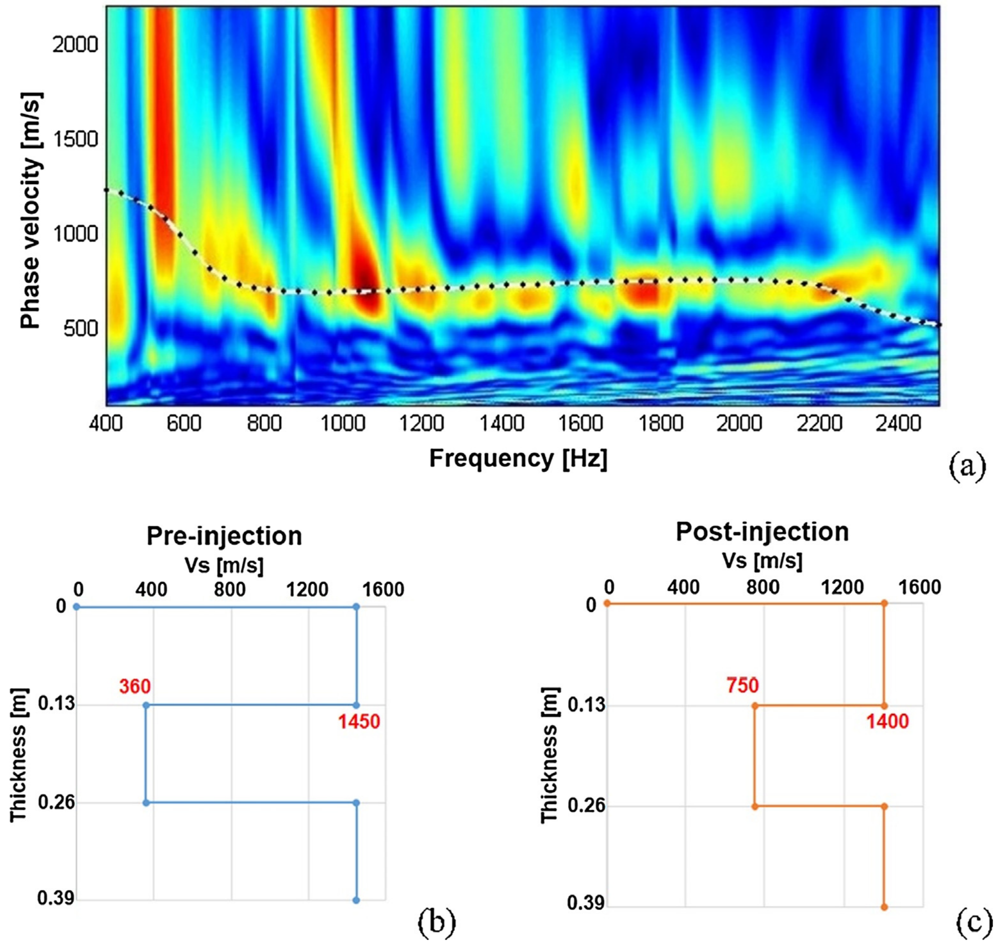

Fig. 13. Results of MASW method applied to P2-B specimen: (a) example of dispersion curve before injection; shear wave velocity models obtained from surface wave velocity before (b) and after (c) core injection.

Computing P-wave velocities as the average of the three-layer structure gave values of about 1800 and 2000 m/s for pre- and post-injected conditions. These results were comparable with those obtained by direct tests, for both single-brick material (see Table 4) and pre/post-injection phases (Table 5).

3.2. Tomography

Tomography applied to wall sections (both horizontal and vertical) processed a combination of a high number of wave paths crossing the investigated areas, by means of ideal rays of various inclinations (paths orthogonal to wall faces belonging to direct tests were included in the data set) (Fig. 5). These data were processed by RUs with their own tools after the section area had been subdivided into a mesh of pixels, and then processed for comparisons with Surfer® mapping software (in the following, contour maps refer to the same range of velocities for all RUs).

Comparison of results obtained at the lowest horizontal section of panel P1-M (RU2), at the highest one in panel P2-B (RU1), and at the mean one of panel P3-S (RU3) are shown in Fig. 14, according to the meshes shown in Fig. 5.

Results for panel P1-M before injection identified high velocities near the steel rod (about 7200 m/s) inserted in the timber element (1625 m/s). Unlike direct test results, the PVC pipe was clearly visible: reduced velocities in that area (around 400 m/s) were measured. After injection, a general but not homogeneous increase in velocities was detected. The area occupied by the PVC pipe seemed to be reduced and, in fact, due to the effect of injections, a definite increase of 400–600 m/s was recorded around the pipe. The inner core showed more uniform distribution of velocities, which stabilized around 3000–3500 m/s; no significant changes were observed around the timber element.

In panel P2-B, transverse high-density brick headers were clearly located with respect to the incoherent core in the pre-injection phase, at a velocity of 3200 m/s (a lower value, 1600 m/s, was measured in the core of the wall). In the post-injection condition, homogenization of section density provided by grouting could no longer distinguish them, as expected for successful intervention. As confirmation, the map of increased velocities before and after injections clearly showed that the grout was distributed correctly in the core of the wall, with a maximum increase in velocity of 50%.

In panel P3-S, the pre-injection tomography map showed high velocity areas (values between 4500 and 5000 m/s) on the left, where the stone leaves were solidly connected. In addition, limited, isolated high-velocity areas (3500–5000 m/s) were detected along the perimeter of the section (2000–3800 m/s). This discontinuity was due to the great irregularity of the stone units in this coarse stone masonry: the unconsolidated core area (velocity values of 300–1800 m/s) extended up to the perimeter in the center of the wall, where the highest core velocities (3500–4800 m/s) were measured after consolidation.

Fig. 15 shows the results of sonic tomography applied by RU1 and RU3 on the vertical section of panel P1-M before and after

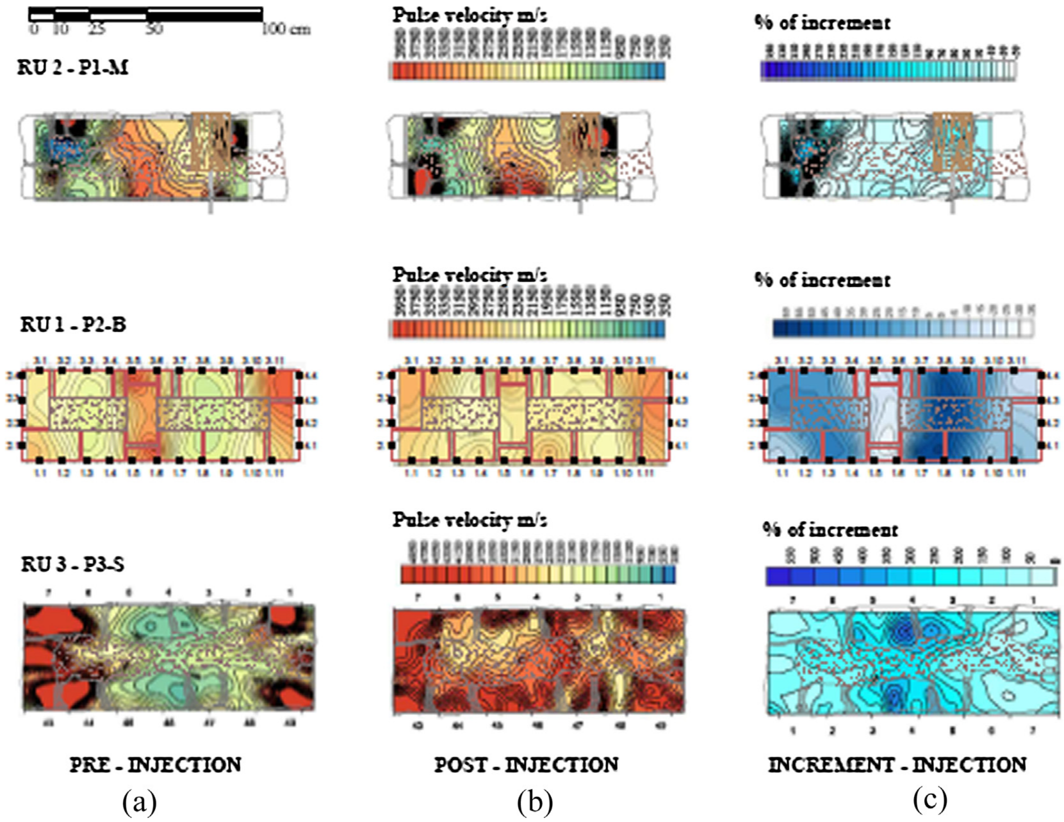

Fig. 14. Tomography velocity maps of representative horizontal sections from panels: pre-injection (a) and post-injection (b) contour maps, and increased ratio after injection (c).

grout injection (only the lower portion below the brick courses was consolidated). Results confirmed the effectiveness of the consolidation intervention. Any changes (increases) in velocity in the upper part of the wall were due to changes in the mean signal velocity because of slight compaction of the loose core material, probably due to vibrations during drilling the injection holes in the specimen.

4. Conclusions

An extensive experimental campaign was carried out on three-leaf panels representative of existing masonry types subjected to elastic wave transmission tests with various acquisition systems and data processing tools. The panels were subjected to compression (P-type) and surface (Lamb-Rayleigh) waves by applying sonic and MASW tests, respectively. The specimens were studied in various configurations: (i) direct tests distributed on the main faces of the panels, (ii) tomography applied to horizontal and vertical panel sections, (iii) surface wave transmission tests along diagonals of panels. This study also established a framework for quantitative evaluation of the sonic pulse velocity characterizing various conditions detectable in representative masonry types. Results showed that:

- Sonic tests are confirmed as effective in detecting large variations in the density of materials inside walls. In particular, differences in material type (e.g., brick courses with respect to multi-layer structures with incoherent cores, transverse elements acting as shear stones, inner incoherent cores), were clearly detectable with direct tests.
- Smaller inclusions can be identified, although still approximately, when crossed by tomographic sections or immersed in a high-density matrix, as in the case of effective consolidation of their surrounding incoherent material with grout injections. Nonetheless, more comprehensive processing of the extended tomographic results reported here will better clarify some aspects which are still difficult to interpret, particularly in the case of small density variations in coupled materials and/or conditions.
- Direct tests provided average values of sonic velocities representative of the various constructive materials (e.g., full brick or stone section, timber element, transverse headers, inner rubble core), with a good approximation among RUs. The reliability of results increased for averages computed on multiple measures in the same area (maximum CoV lower than 40%), thus revealing the significant accuracy of low-frequency waves to define inhomogeneous media.
- Both direct and tomographic tests confirmed their high reliability in quantifying the effectiveness of grout injections to homogenize consolidated inner cores with outer leaves: the increase in sonic velocity detected in the panels with respect to pre-injection conditions ranged from 15 to 30% for P1-M, 30–60% for P2-B, and from 2 to 3.5 times for P3-S (average CoV among RUs of about 20%). Tomographic results were also consistent with the grout quantities migrating across the void distribution, which were estimated on the walls during the injection phase: comparing the two panels in which the complete inner cores were injected, i.e., P2-B and P3-S, with about 16% and 38% of voids, respectively, velocity increases after injections (average values among all RUs) were 54% for the brick wall and 187% for the stone one.

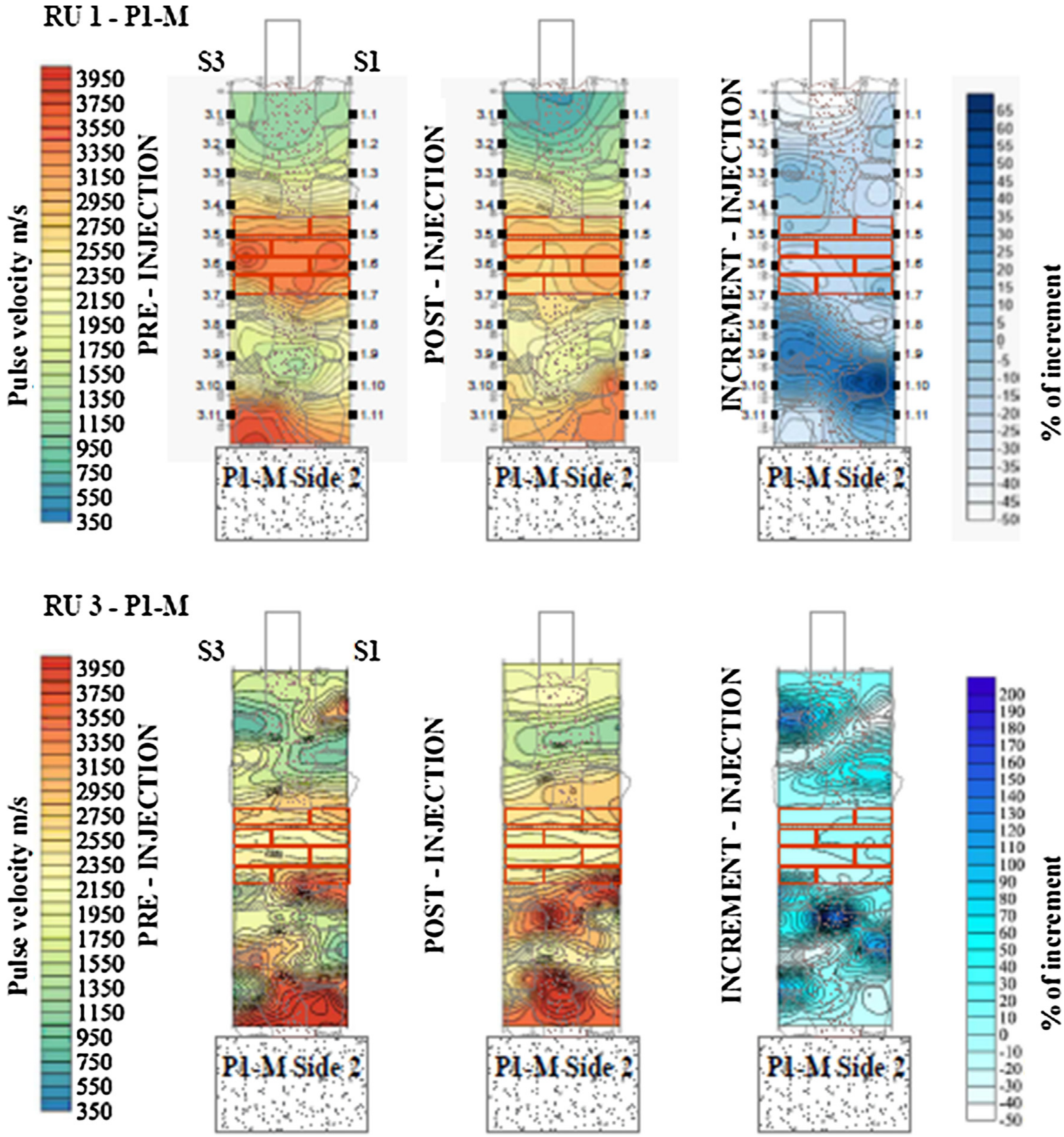

Fig. 15. Tomographic velocity maps of vertical section from panel P1-M: comparison between pre- and post-injection contour maps, and increased ratio after injection.

- The surface wave transmission method was also effective in identifying the layered internal structure of the wall and the improvements provided by injection. The conversion of recorded velocity values into P-wave velocities matched the results of sonic test outcomes for panel P2-B: compared with the average of sonic velocity computed for all RUs, MASW results were slightly lower (about 20% and 6% for pre- and post-injection velocity values, respectively). The applicability of this method depends on the possibility of surveying a wall section which is twice as long as the wall thickness. In terms of working time, although the MASW method is comparable to direct tests, it is much faster than tomography.
- Results were comparable among the different RUs involved in this research, although different acquisition systems and equipment as well as processing tools were adopted. Further processing of the huge dataset of wave signals recorded in this study will provide better understanding of correlations among wave parameters, material properties, and the dimensions and types of inclusions.

This research validated different methods applied in various conditions to experimental models for the extension of wave transmission tests to several masonry types detectable in historic constructions. The method remains qualitative for highly heterogeneous materials, although relationships with mechanical properties can be evaluated by collecting results obtained in various contexts and material conditions.

Conflict of interest

None.

Acknowledgments

The authors would like to thank the CPIPE Building School of Camin (Padova) for its assistance in constructing the specimens; Kerakoll SpA and S. Anselmo Furnace SpA for providing the mortar and grout, and the bricks, respectively; V. dal Farra for collaboration in finding stone materials and in assisting during the injection phase. L. Rosato and A.G. Mandrini (University of Padova), E. Gabrielli, C. Ciani, and F. Berardi (University of Bologna), G. Pappadà (Politecnico di Milano), and M. Cucchi and C. Tiraboschi (Laboratory of Materials Testing of the Politecnico di Milano), are also gratefully thanked for their assistance in the acquisition and processing phases.

Funding

This work was funded by the Department of Cultural Heritage of the University of Padova [project fund 2016]; partial funding was also available from DPC-ReLuis [Executive Project 2017 and 2018: Masonry Constructions].

References

[1] Aerojet General Corporation, Investigation on sonic testing of masonry walls, Final Report, Dept. of General Services of Architecture and Construction, California, US, 1967.
[2] ASTM C939-10 Standard Test Method for Flow of Grout, ASTM International, 2010.
[3] M. Berra, L. Binda, L. Anti, A. Fatticcioni, Non destructive evaluation of the efficacy of masonry strengthening by grouting techniques, in: Proc. Int. Workshop Effectiveness of Injection Techniques for Retrofitting of Stone and Brick Masonry Walls in Seismic Areas, 1992, pp. 63–70.
[4] L. Binda, Investigation for the diagnosis of historic buildings: application at different scales, in: Proc. Seminario a Intervençao no Patrimonio Praticas de Conservaçao e Reabilitaçao, Portugal, 2005.
[5] L. Binda, L. Cantini, G. Cardani, A. Saisi, C. Tiraboschi, Use of flat-jack and sonic tests for the qualification of historic masonry, in: Proc. North American Conf., US, 2007, pp. 791–803.
[6] L. Binda, L. Cantini, P. Condoleo, A. Saisi, L. Zanzi, Investigation on the pillars of the Syracuse cathedral in Sicily, in: Proc. Int. Conf. Structural Faults & Repair, UK, 2006.
[7] L. Binda, A. Saisi, C. Tiraboschi, Investigation procedures for the diagnosis of historic masonries, J. Constr. Build. Mater. (2000) 199–233.
[8] L. Binda, A. Saisi, C. Tiraboschi, S. Valle, C. Colla, M. Forde, Application of sonic and radar tests on the piers and walls of the Cathedral of Noto, Constr. Build. Mater. 17 (8) (2003) 613–627.
[9] L. Binda, A. Saisi, L. Zanzi, Sonic tomography and flat-jack tests as complementary investigation procedures for the stone pillars of the temple of S. Nicolò l'Arena (Italy), J. NDT&E Int. 36 (2003) 215–227.
[10] L. Cantini, R. Felicetti, L. Zanzi, S. Munda, M. Meana, L. Binda, Sonic tomography applied to historic masonry structures: validation of the testing methodology and of the data elaboration by different computer codes, in: Proc. Int. Conf. Structural Faults & Repair, UK, 2012.
[11] G. Cardani, L. Binda, Guidelines for the evaluation of the load-bearing masonry quality in built heritage, in: Proc. Int. Conf. Built Heritage: Monitoring Conservation Management, 2015, pp. 127–140.
[12] F. Casarin, F. da Porto, M.R. Valluzzi, C. Modena, Evaluation of the structural behavior of historic masonry buildings by using sonic pulse velocity method, in: Int. Conf. on Structural Studies, Repairs and Maintenance of Heritage Architecture, Czech Republic, 2007, pp. 227–236.
[13] E. Cescatti, R. Deiana, L. Rosato, C. Modena, Evaluation of injection intervention on a real case in a medieval complex, in: 12th North American Masonry Conference, US, 2015, pp. 11.
[14] E. Cescatti, L. Rosato, M.R. Valluzzi, F. Casarin, An automatic algorithm for the execution and elaboration of sonic pulse velocity tests in direct and tomographic arrangements, in: R. Aguilar, D. Torrealva, S. Moreira, M.A. Pando, L.F. Ramos L.F. (Eds.) Structural Analysis of Historical Constructions. An Interdisciplinary Approach. RILEM Bookseries, vol. 18, pp. 716–724. Springer, Cham. Proc. of SAHC 2018 – 11th International Conference on Structural Analysis of Historical Constructions, Cusco (Peru), 11–13 September, 2018. https://doi.org/10.1007/978-3-319-99441-3_77.
[15] C. Colla, Comparative testing for improved diagnosis of historic structures, in: M. Krüger (Ed.), EWCHP-2011, European Workshop on Cultural Heritage Preservation, Fraunhofer IRB Verlag, Berlin, 2011, pp. 140–147.
[16] C. Colla, P.C. Das, D. McCann, M.C. Forde, Sonic, electromagnetic & Impulse radar investigation of stone masonry bridges, J. NDT&E Int. 30 (4) (1997) 249–254.
[17] C. Colla, G. Pascale, Non-destructive and minor-destructive tests for masonry characterization of the Ghirlandina tower in Modena, in: R. Cadignani (Ed.), La torre Ghirlandina – storia e restauro, Italy, 2010, pp. 218–227.
[18] M.C. Forde, K.F. Birjandi, A.J. Batchelor, Fault detection in stone masonry bridges by non-destructive testing, in: Proc. Int. Conf. Structural Faults & Repair, UK, 1985, pp. 373–379.
[19] Y.H. Lee, T. Oh, The simple lamb wave analysis to characterize concrete wide beams by the practical MASW test, Materials 9 (2016) 437.
[20] V. Luprano, C. Colla, Ultrasonic and sonic techniques applied to concrete and masonry structures, in: C. Meola (Ed.), Recent Advances in Non-Destructive Inspection, Nova Science Publishers Inc, New York, 2010, pp. 59–88.
[21] L. Miranda, L. Cantini, J. Guedes, L. Binda, A. Costa, Applications of sonic tests to masonry elements: influence of joints on the propagation velocity of elastic waves, J. Mater. Civ. Eng. 25 (2013) 667–682, https://doi.org/10.1061/(ASCE)MT.1943-5533.0000547.
[22] J.L. Noland, R.H. Atkinson, J.C. Baur, An investigation into methods of nondestructive evaluation of masonry structures, Report to the National Science Foundation, National Technical Information Service Report No. PB 82218074, US, 1982.
[23] Onsiteformasonry – On-site investigation techniques for the structural evaluation of historic masonry buildings, EC Project FP5 EESD, EVK4-CT-2001-00060, 2005 (CD-ROM).
[24] T.C. Rilem, 127-MS, MS.D.1 Measurement of mechanical pulse velocity for masonry, J. Mater. Struct. 29 (1996) 463–466.
[25] G. Riva, C. Bettio, C. Modena, The use of sonic wave technique for estimating the efficiency of masonry consolidation by injection, in: Proc. Int. Brick/Block Masonry Conf., China, 1997, pp. 28–39.
[26] M. Schuller, M. Berra, A. Fatticcioni, R. Atkinson, L. Binda, Use of tomography for diagnosis and control of masonry repairs, in: Proc. Int. Brick/Block Masonry Conf., Canada, 1994, pp. 438–447.
[27] B. Silva, M. Dalla Benetta, F. Da Porto, M.R. Valluzzi, Compression and sonic tests to assess effectiveness of grout injection on three-leaf stone masonry walls, Int. J. Arch. Heritage 8 (3) (2014) 408–435, https://doi.org/10.1080/15583058.2013.826300.
[28] L.V. Socco, S. Foti, D. Boiero, Surface-wave analysis for building near-surface velocity models – Established approaches and new perspectives, Geophysics 75 (5) (2010) 75A83–75A102, https://doi.org/10.1190/1.3479491.
[29] L.V. Socco, C. Strobbia, Surface-wave method for near-surface characterization: a tutorial, Near Surf. Geophys. 2 (2004) 165–185, https://doi.org/10.3997/1873-0604.2004015.
[30] M.R. Valluzzi, F. da Porto, C. Modena, Grout requirements for the injection of stone masonry walls, in: Proc. Int. Conf. Performance of Construction Materials in the New Millennium, Egypt, 2003, I, pp. 393–402.
[31] M.R. Valluzzi, F. da Porto, C. Modena, Behavior and modeling of strengthened three-leaf stone masonry walls, J. Mater. Struct. 37 (2004) 184–192, https://doi.org/10.1007/BF02481618.
[32] M.R. Valluzzi, F. da Porto, F. Casarin, N. Monteforte, C. Modena, A contribution to the characterization of masonry typologies by using sonic waves investigations, in: Proc. Int. Symp Non Destructive Testing in Civil Eng., France, 2009, pp. 713–718.
[33] M.R. Valluzzi, N. Mazzon, M. Munari, F. Casarin, C. Modena, Effectiveness of injections evaluated by sonic tests on reduced scale multi-leaf masonry building subjected to seismic actions, in: Proc. Int. Symp. Non Destructive Testing in Civil Eng., France, 2009, pp. 677–682.
[34] M.R. Valluzzi, Conservation of historical constructions in seismic area: experimental research on enhancement techniques for masonry buildings, in: Proc. Int. Conf. Advances in Construction Materials and Systems, India, 2017, 1, pp. 139–153.